Detectability of Magma-Sediment Alteration Mineralogy Via Multi-Instrument Analysis: Implications for Terrestrial Analogs and the Search for Potentially Habitable Environments on Mars. J.R. Crandall[1], J. Filiberto[2], S.P. Schwenzer[3], and S.M. Rimmer[4]. [1]Eastern Illinois University, Department of Geology & Geography, 600 Lincoln Ave., Charleston, IL 61920, USA (Jrcrandall@eiu.edu). [2]ARES, NASA Johnson Space Centre, 2101 E NASA Pkwy, Houston, TX 77058, USA. [3]AstrobiologyOU, EEES, The Open University, Walton Hall, Milton Keynes MK7 6AA, UK. [4]Southern Illinois University Carbondale, School of Earth Systems and Sustainability, 1259 Lincoln Drive, Carbondale, IL 62901, USA.

Introduction: The detection of magmatically driven hydrothermal systems on Mars has met with limited success. Remote sensing efforts have detected limited exposures, though they are usually isolated occurrences, and do not necessarily represent an in-situ alteration sequence [1-6]. Some of the best evidence for such a system comes from Mars Exploration Rover Spirit's investigations of Gusev Crater. Diverse alteration minerals were investigated, including possible detections of amorphous silica and montmorillonite [7,8]. The question remains whether remote sensing/spectroscopy alone is capable of detecting such an alteration front, or if more detailed in-situ analyses are required. In order to constrain this, we have used Mars relevant instrumentation to investigate a terrestrial analog on the Colorado Plateau where a mafic dike intrudes the Jurassic Curtis Sandstone.

Field Site Geology: The San Rafael Swell, Utah, USA hosts a ~60km long and 30km wide mafic dike swarm and associated sills and breccias that intruded into the Jurassic San Rafael Group from approximately 4.6-3.7 Ma [9-11]. In addition to work done on other dikes in this area [12-14], the samples in this study were collected from the upper Jurassic Curtis Sandstone, a subarkosic, weakly dolomite cemented sandstone that is well exposed in the area [15,16]. While quartz sandstones have not been detected on Mars, the choice of a relatively mineralogically uniform and non-reactive sandstone allow for a dominance of the geochemical fingerprint of the basalt, and therefore straightforward comparisons between analytical methods and results, as well as the avoidance complications that arise in multiple mineral systems.

Methods: Samples of the altered Curtis Sandstone were collected across the outcrop of host rock and the intrusion to represent a "cross-section" with respect to distance from the dike (Figure 1). A distal sample (RS) of relatively unaltered Curtis Sandstone was also collected a significant distance from the dike. The mineralogy of all samples was constrained via VNIR (ASD TerraSpec Pro) analyses and multiple XRD (Rigaku Ultima IV) analyses. The XRD analyses include bulk, unoriented clay aggregate, and oriented clay fraction (2μm), and are summarized in Table 1.

Figure 1: *Basaltic dike intruding the Curtis Sandstone at the field site. Approximate cross-sectional sampling was completed to the right of the photographed section where the Curtis provides a thicker cross-sectional area.*

VNIR Results: While VNIR does not detect quartz or feldspar due to wavelength limitations, detections throughout the "cross-section" closely mirror the oriented clay fraction XRD detections, and show that with increasing proximity to the dike, significant mineralogical changes can be observed with respect to the "unaltered" sample (Table 1). The reflectance minima and maxima in sample RS are consistent with the detection of Fe/Mg chlorite and muscovite mica. Owing to the sedimentary origin of the Curtis Sandstone, these particular phyllosilicates are likely of sedimentary origin, and indicate that the sampling distance from the dike was sufficient to avoid the alteration aureole.

At the physical contact between the dike and the Curtis Sandstone, CD-1 contains gypsum, the only sulfate detected in the system, and phengite. A few inches from the contact, the dominant mineralogy shifts to montmorillonite and calcite in CD-2. CD-3, a few feet from the contact, also contains Montmorillonite and Calcite, along with the addition of Siderite. Three to four feet from the contact in CD-4, montmorillonite and siderite continue to be detected, but calcite gives way to ankerite.

Sample	Description	VNIR Mineralogy	XRD Bulk Analysis Mineralogy and Estimated Weight Percent	XRD Oriented Clay Fraction Analysis Mineralogy
RS	Roadside grab-bag, unaltered	Chlorite Fe/Mg, Muscovite	Quartz: 60.3% Calcite: 24.69% Bytownite: 15.1%	Chlorite
CD-1	Contact between Curtis and dike	Gypsum, Phengite	Quartz: 84.9% Albite lo: 11.3% Calcite: 3.9%	Montmorillonite/Smectite
CD-2	Near contact, further up-section	Montmorillonite, Calcite	Quartz: 66.9% Calcite:16.6% Albite hi: 5.3% Bytownite: 4.3%	Montmorillonite Amorphous Phase
CD-3	Curtis 1-2 feet from dike	Montmorillonite, Calcite, Siderite	Quartz: 67% Labradorite: 18.8% Calcite: 14.2%	Montmorillonite/Smectite
CD-4	Curtis 3-4 feet from dike	Montmorillonite, Ankerite, Siderite	Quartz: 83.6% Calcite: 14.1% Euclase: 1.2% Altisite: 1.1%	Montmorillonite Chlorite

Table 1: *Sample description, and detected mineralogy for VNIR, bulk, and oriented clay fraction XRD analyses.*

XRD Results: Bulk XRD analyses detected quartz, calcite, and felspar in every sample, as expected given the composition of the Curtis Sandstone (Figure 2). Strong quartz and calcite detections were manually confirmed, while the remainder of species were identified with JADE software. We interpret the various silicate species detected by JADE to be minor feldspars whose signal has been overwhelmed by the dominant signals of quartz and calcite in each sample. Besides calcite, bulk XRD and VNIR analyses produce unique detections.

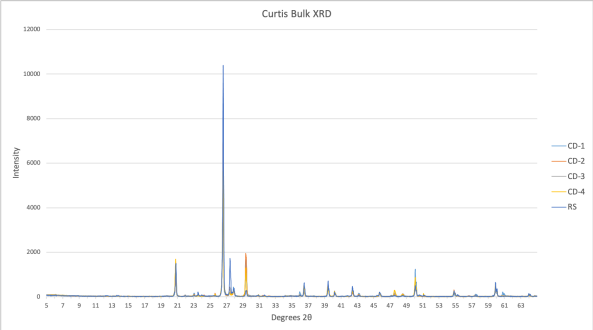

Figure 2: *Bulk XRD analyses for "cross section" samples stacked to highlight similarities and differences with respect to alteration mineralogy.*

Oriented clay fraction analyses have significant overlap with VNIR detections. Chlorite is detected far from the contact in RS, and 3-4 feet away from the contact in CD-4, but gives way to montmorillonite/smectite with increased proximity to the dike. Of note is the detection of an amorphous phase in CD-2.

Conclusions: Bulk XRD analyses were critical to establish the dominant mineralogy of the system, though additional methods were required to investigate the nature of the hydrothermal alteration assemblage. Although distinct from the bulk XRD detections, the VNIR and oriented clay fraction XRD detections had a strong overlap, and allowed for a more detailed description of the hydrothermal alteration mineralogy. The unifying feature across all analytical methods is that higher temperature minerals are detected proximal to the dike, while lower temperature minerals are detected in the more distal and unaltered samples. Of particular note is the detection of an amorphous phase in CD-2, which along with montmorillonite bears resemblance to sites on Mars ranging from Gusev to Gale and Jezero craters [17-19]. Furthermore, the occurrence of sulfates and carbonates is a very important consideration on Mars for processes of post-impact high temperature such as investigated here, and low temperature alteration and evaporation [20-22]. The latter opens up a wider range of questions for this study of remote observability. When viewed independently, the differences in detection limits and resolution between analytical methods confirms the difficulty of identifying these systems remotely. To positively identify and constrain magmatically induced hydrothermal systems on Mars, it is likely that a combination of remote and in-situ analyses will be required.

Acknowledgements: We would like to thank National Geographic Society's Committee for Research and Exploration for funding the field expedition, as well as acknowledge support from NASA PSTAR and Research England's grant 'Expanding Excellence in England' 124.18.

References: [1] Skok J. et al., (2010) *Nat. Geosci. 3(12): 838.* [2] Milliken R.R. et al., (2008) *Geology 36(11): 847-850.* [3] Filiberto J. et al., (2019) *Volatiles in the Martian Crust 13-33.* [4] Viviano C.E. et al., (2013) *JGR: Planets 118(9), 1858-1872.* [5] Ehlmann B.L and Edwards C.S. (2014) *Annu. Rev. Earth Planet Sci. 42, 291-315.* [6] Semprich J. et al. (2019) *JGR: Planets 124(3), 681-702.* [7] Ruff S.W. et al., (2011) *JGR 116: E7.* [8] Carter J. and Poulet F. (2012) *Icarus 219(1):250-253.* [9] Gilluly J. (1927) *Am. J. Sci. 14, 199-211.* [10] Delaney P.T and Gartner A.E. (1997) *GSA Bull. 109, 1177-1192.* [11] Kiyosugi K. et al., (2012) *Geology 40, 695-698.* [12] Costello L.J. et al., (2020) *Geochem. 80, 125613.* [13] Crandall J.R. et al., (2021) *PSJ 2, 138.* [14] Slank R.A. et al., (2023) *LPSC #1723.* [15] Smith J.F. et al., (1963) *USGS Prof. Paper 363: 102.* [16] Kreisa R.D. and Moiola R.J. (1986) *GSA Bull. 97:381-387.* [17] Rowe M.C and Brewer B.J. (2018) *Comput. Geosci. 120:21-31.* [18] Clark B.C. et al., (2007) *JGR 112, E6.* [19] Clevé E. et al., (2003) *JGR: Planets 128,6.* [20] Bridges J.C. (2019) *Volatiles in the Martian Crust 89-118.* [21] Rapin W. et al., (2019) *Nat. Geosci.12, 839-895.* [22] Sutter B. et al., (2017) *JGR: Planets 112,12.*